NUMERICAL MODELING FOR 3D ACOUSTIC WAVE EQUATION IN THE FREQUENCY DOMAIN

TAEYOUNG HA[1], YUNSEOK CHOI[2]*, CHANGSOO SHIN[3], DONG-JOO MIN[3]

[1] *National Institute for Mathematical Sciences, 385-16, Doryong-dong, Yuseong-gu, Daejeon 305-340, South Korea. tha@nims.re.kr*
[2] *Korea Ocean Research and Development Institute, Ansan, P.O. Box 29, Seoul 425-600, South Korea. choi76@kordi.re.kr*
[3] *Department of Energy Resources Engineering, Seoul National University, 599 Gwanangno, Gwanak-gu, Seoul 151-744, South Korea.*
* *Corresponding author*

(Received April 4, 2008; revised version accepted September 8, 2008)

ABSTRACT

Ha, T., Choi, Y., Shin, C.S. and Min, D.-J., 2009. Numerical modeling for 3D acoustic wave equation in the frequency domain. *Journal of Seismic Exploration*, 18: 57-79.

We investigate a frequency-domain finite-element method for three-dimensional modeling of the acoustic wave equation. Frequency-domain modeling has several advantages over time-domain modeling, even though it requires huge computational memory compared to time-domain modeling. One of these advantages is that multi-shot modeling can be performed more efficiently in the frequency domain than in the time domain, and another is the ability to work on a frequency-by-frequency basis, which makes it possible to distribute frequencies across processors. Considering that frequency-domain modeling is popular in waveform inversion because of source wavelet estimation and multi-shot modeling, 3D frequency-domain finite-element modeling can be effectively used in 3D waveform inversion. We derive a numerical dispersion relationship for the 3D frequency-domain finite-element method and then analyze numerical dispersion on the basis of dispersion curves. From the dispersion analysis, we determine the minimum number of grid points per wavelength. The validity of the 3D finite-element modeling algorithm is examined for a three-layered model and the SEG/EAGE salt model.

KEY WORDS: 3D modeling, acoustic wave equation, frequency-domain, finite-element, numerical dispersion.

0963-0651/09/$5.00

INTRODUCTION

Several numerical methods have become standard tools for seismic migration, modeling, and inversion. These technologies are frequently based on finite differences, pseudo-spectral techniques, boundary elements, prolate spheroidal wave functions and occasionally finite elements (Claerbout, 1971; Kelly et al., 1976; Marfurt, 1984; Reshef et al., 1988; Carcione et al., 2002; Beylkin and Sandberg, 2005). It is clear that, of these, the finite element approach is not the most popular. Far fewer papers have been published on this subject than on almost any of the other techniques. Primarily because of the enormous size of the matrix inversion problem required to accurately implement this methodology, frequency-domain finite element techniques have found little use in three dimensions. In contrast, finite difference methods have become one of the more dominant techniques for precisely the opposite reason. Space-time-finite-differences are relatively easy to parallelize and execute on large modern cluster computers. Although transform methods, including pseudo-spectral and more recently prolate-spheroidal methods, usually have an advantage in both accuracy and stability, they are generally more difficult to implement than finite-differences and so have not enjoyed wide use in 3D seismic modeling or wavefield inversion.

Three-dimensional-space-time numerical modeling is fairly easy to implement. Even when individual cluster-computer nodes have significant memory limitations, domain decomposition can effectively solve problems of almost any size. While domain decomposition requires a stable and fast network, careful programming mitigates communication by coupling double-buffering with careful data transfers during extensive computations. From a single synthesis point of view, the only serious issue with regards to space-time algorithms is the fact that maintaining stability requires tiny evolutionary time-steps and consequently results in very large computational demands. Three-dimensional synthesis of a single reasonably large artificial seismic survey is rapidly becoming within reach of modern cluster-computer environments. If the focus is on full waveform adjoint-state inversion, the situation changes dramatically. Synthesis of a single survey is not sufficient to produce a solution of the posed inverse problem. Iteratively estimating source wavelets is complicated by the need to unwrap phases and consequently usually requires forward and backward transformation between time and frequency. Time domain convolutions require more resources than frequency domain multiplications. Computation of multiple approximate inverse Hessians, partial-derivative wavefields, source wavelet estimation, and backward-propagated residuals over a broad spectral range renders 3D space-time inversion virtually impossible to perform.

Finite-element-frequency-domain modeling has several potentially significant advantages over space-time finite difference or transform methods.

One of the most important is that the entire modeling algorithm can, in theory, be posed so that data is synthesized for all shots at once. Another practical advantage is the ability to work on a frequency-by-frequency basis. Matrix inversions at one frequency can be extrapolated to inversions at the next. The fact that one need not use every frequency (Pratt et al., 1998; Shin and Min, 2006) implies the potential for very efficient solutions of very difficult 3D inversion problems. Once the appropriate computations are complete, calculating steepest descent directions and source wavelets (Shin et al., 2001; Shin and Min, 2006) in both logarithmic and traditional least squares is fairly straightforward. A third and perhaps more esoteric advantage lies in the ability to formulate acoustic, elastic, and coupled acoustic-elastic modeling and inversion algorithms within the same general scheme. Once the complex-impedance matrix formulation is available, the route to modeling and inversion is clearly defined and virtually identically in operation.

By far the biggest disadvantage of the frequency-domain technique arises from the phrase "once the appropriate computations are complete." The computational and storage resources (fast as well as slow disk) required to invert the resulting matrix-like equations and complete the "appropriate computations" is truly enormous. A secondary issue is the fact that the higher order finite element method results in a parasitic dispersion analysis mode (Belytschko and Mullen, 1978), but this is completely swamped by the resources required to solve the complex-impedance matrix equations.

We believe that 3D-frequency-domain-finite-element formulation of wave equation synthesis is of significant potential value and worthy of considerable study. Nevertheless, because of the severe computational limits imposed by available hardware and software, initial steps must be somewhat limited. Consequently in the following sections, we focus on the 3D acoustic equation and exploit the Galerkin (variational) approximation procedure to derive the complex-impedance matrix equation specifying a full 3D finite element modeling algorithm. We derive the appropriate dispersion analysis endemic to specifying accurate boundary conditions and demonstrate the feasibility of 3D frequency domain finite-element modeling by displaying low frequency synthetic seismograms for the SEG/EAGE 3D model.

GOVERNING EQUATION AND FINITE ELEMENT METHOD

Governing equation

For our purposes, the three dimensional scalar wave equation in time-domain is given by

$$[1/v(\mathbf{x})^2][\partial^2 u(\mathbf{x},t)/\partial t^2] - \nabla^2 u(\mathbf{x},t) = f(\mathbf{x},t) \quad , \tag{1}$$

where

$$\nabla^2 u(\mathbf{x}) = [\partial^2 u(\mathbf{x})/\partial x^2] + [\partial^2 u(\mathbf{x})/\partial y^2] + [\partial^2 u(\mathbf{x})/\partial z^2] \quad ,$$

and $u(\mathbf{x})$ is the pressure, $v(\mathbf{x})$ is the sound speed, and $f(\mathbf{x},t)$ is the impulsive force. Taking the Fourier transformation of eq. (1) yields

$$-[\omega^2/v(\mathbf{x})^2]\tilde{u}(\mathbf{x},\omega) - \nabla^2\tilde{u}(\mathbf{x},\omega) = \tilde{f}(\mathbf{x},\omega) \quad , \tag{2}$$

where

$$\tilde{u}(\mathbf{x},\omega) = \int_{-\infty}^{\infty} u(\mathbf{x},t)e^{-i\omega t}dt \quad ,$$

$$\tilde{f}(\mathbf{x},\omega) = \int_{-\infty}^{\infty} f(\mathbf{x},t)e^{-i\omega t}dt \quad .$$

Weak formulation in Helmholtz equation

In a bounded computational domain, equation (1) becomes

$$-[\omega^2/v(\mathbf{x})^2]\tilde{u}(\mathbf{x},\omega) - \nabla^2\tilde{u}(\mathbf{x},\omega) = \tilde{f}(\mathbf{x},\omega) \quad , \quad \text{in } \Omega \tag{3a}$$

$$\tilde{\mathbf{B}}_j\tilde{u}(\mathbf{x},\omega) = 0 \quad , \quad \text{in } \Gamma \tag{3b}$$

where $\tilde{\mathbf{B}}_j$, $j = 1,2,3$ are given (Clayton and Engquist, 1977) by eq. (A-9) in Appendix A. For our numerical experiments, we use the second order absorbing boundary condition specified by $\tilde{\mathbf{B}}_2$. The weak formulation of eq. (3) is

$$-\omega^2 \int_\Omega [1/v(\mathbf{x})^2]\tilde{u}(\mathbf{x},\omega)\varphi(\mathbf{x})d\mathbf{x} + \int_\Omega [1/v(\mathbf{x})^2]\nabla\tilde{u}(\mathbf{x},\omega)\cdot\nabla\varphi(\mathbf{x})d\mathbf{x}$$

$$+ \int_\Gamma \mathbf{P}_\Gamma\mathbf{u}(\mathbf{x})\varphi(\mathbf{x})d\Gamma = \int_\Omega f(\mathbf{x},\omega)\varphi(\mathbf{x})d\mathbf{x} \quad , \tag{4}$$

where $\varphi(\mathbf{x})$ is a weighting function and

$$\nabla u(\mathbf{x}) = \{[\partial u(\mathbf{x})/\partial x],[\partial u(\mathbf{x})/\partial y],[\partial u(\mathbf{x})/\partial z]\} \quad ,$$

and $\mathbf{P}_\Gamma$ is determined from the boundary condition $\tilde{\mathbf{B}}_2$. For example, suppose the computational domain is $[0,x_{max}]\times[0,y_{max}]\times[0,z_{max}]$. From eq. (A-9b), $\mathbf{P}_\Gamma\mathbf{u}(\mathbf{x})$ on the surface $z = z_{max}$ is

$$\mathbf{P}_\Gamma\mathbf{u} = (i\omega/v)\tilde{\mathbf{u}} + (iv/2\omega)(\tilde{\mathbf{u}}_{xx} + \tilde{\mathbf{u}}_{yy}) \quad . \tag{5}$$

In our numerical simulation, shape functions are linear polynomials, and therefore,

$$\int_{\Gamma} \mathbf{P}_{\Gamma}\mathbf{u}(\mathbf{x})\varphi(\mathbf{x})d\Gamma$$

$$= \int_0^{x_{max}} \int_0^{y_{max}} [(i\omega/v)\tilde{\mathbf{u}}(\mathbf{x}) + (iv/2\omega)(\tilde{\mathbf{u}}_{xx}(\mathbf{x}) + \tilde{\mathbf{u}}_{yy}(\mathbf{x}))]\varphi(\mathbf{x})dxdy$$

$$= \int_0^{x_{max}} \int_0^{y_{max}} [(i\omega/v)\tilde{\mathbf{u}}(\mathbf{x}) - (iv/2\omega)(\tilde{\mathbf{u}}_{x}(\mathbf{x})\varphi_x(\mathbf{x}) + \tilde{\mathbf{u}}_{y}(\mathbf{x})\varphi_y(\mathbf{x}))]dxdy$$

$$= \int_0^{y_{max}} [(iv/2\omega)\tilde{\mathbf{u}}_x(\mathbf{x})\varphi_x(\mathbf{x})]_0\, dy + \int_0^{x_{max}} [(iv/2\omega)\tilde{\mathbf{u}}_y(\mathbf{x})\varphi_y(\mathbf{x})]_0^{y_{max}} dx \quad ,$$

where $[f(\mathbf{x})]_a^b$ means $f(\mathbf{b}) - f(\mathbf{a})$. The standard Galerkin approximation (Marfurt, 1984; Zienkiewicz and Taylor, 2000) yields the discrete system

$$\mathbf{Su} = (\mathbf{K} + \mathbf{M} + \mathbf{C})\mathbf{u} = \mathbf{f} \quad , \tag{6}$$

where the stiffness matrix **K**, the mass matrix **M**, and the damping matrix **C** are given by

$$\mathbf{K} = [k_{ij}] \quad , \quad k_{ij} = \int_{\Omega} \nabla\varphi_i(\mathbf{x})\cdot\nabla\varphi_j(\mathbf{x})d\mathbf{x} \quad ,$$

$$\mathbf{M} = [m_{ij}] \quad , \quad m_{ij} = -\omega^2 \int_{\Omega} [1/v(\mathbf{x})^2]\varphi_i(\mathbf{x})\varphi_j(\mathbf{x})d\mathbf{x} \quad ,$$

$$\mathbf{C} = [c_{ij}] \quad , \quad c_{ij} = -\int_{\Gamma} \mathbf{P}_{\Gamma}\mathbf{u}(\mathbf{x})\varphi(\mathbf{x})d\Gamma \quad .$$

Here, f is the source vector and $\varphi_j(x)$ are shape functions.

Comparison with the analytic solution

The analytic solution of the direct wave and the free surface reflected wave in three dimension (Officer, 1958) are

$$\psi_D = (1/r)f(t - r/c) \quad , \tag{7}$$

$$\psi_{re} = -(1/r')f(t - r'/c) \quad , \tag{8}$$

where f(t) is a source function, r is the distance between source and receiver, r′ is the distance between source and receiver via the reflection path, and c is the velocity as in Fig. 1. The total received signal will then be simply

$$\psi = \psi_D + \psi_{re} = (1/r)f(t - r/c) - (1/r')f(t - r'/c) \quad . \tag{9}$$

Fig. 2 shows a comparison between our 3D acoustic modeling results and analytic solution. For this comparison, we use the first derivative of Gaussian function as source wavelet and locate a source at the depth of 20 m below the free surface and a receiver at the depth of 700 m on the same vertical line with the source position. From Fig. 2, we note that the 3D acoustic modeling solution coincides well with analytic solution. So we assert that our 3D acoustic modeling algorithm has no blemish in theoretical aspects.

The dispersion analysis of 3D acoustic problem concerned with eq. (6) is expressed in Appendix B.

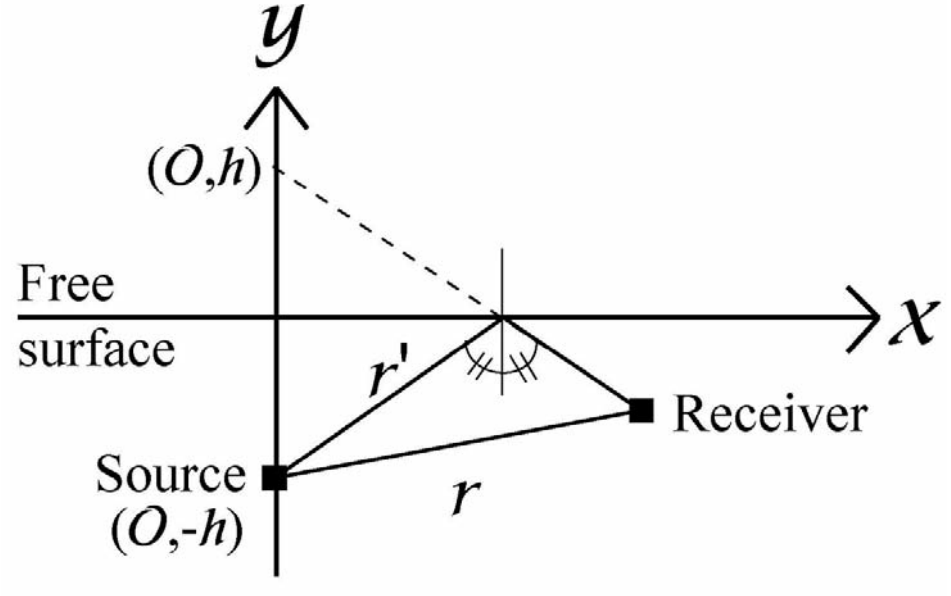

Fig. 1. Wave path from a point source to a receiver in a constant velocity medium bounded by a free surface.

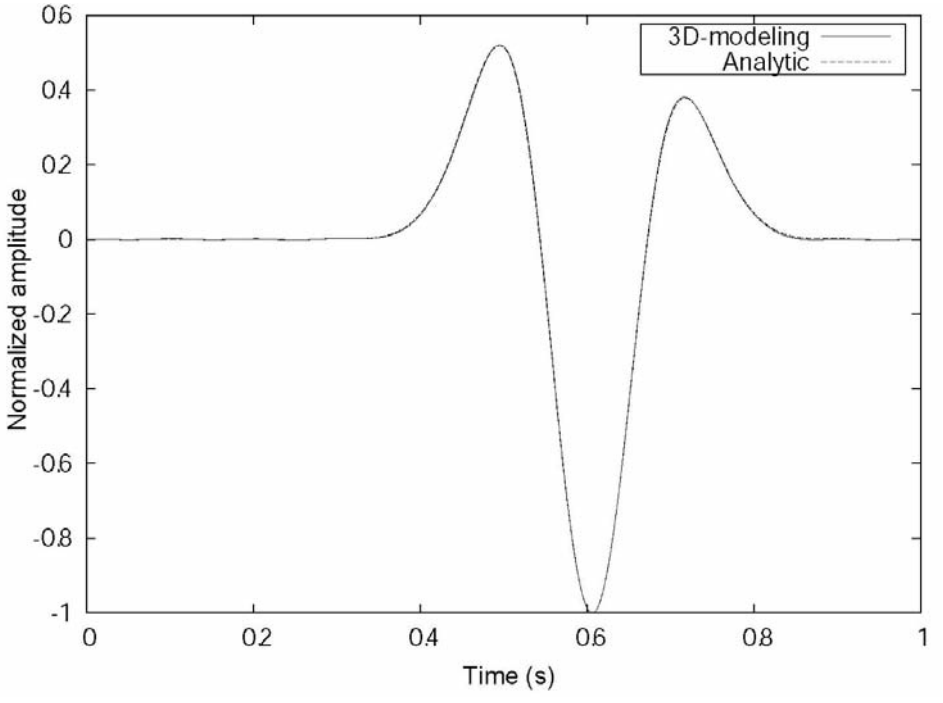

Fig. 2. Comparison between 3D acoustic modeling solution and analytic solution at a receiver placed at the depth of 700 m.

NUMERICAL EXPERIMENTS

Homogeneous model

Our first priority was to test the validity of our code. To do this, we generated data over a simple homogeneous model with a sound speed of 2 km/sec. In our all examples, we divided models by cubes for finite-element formulation and used the first derivative of Gaussian function as source wavelet. With a uniform grid spacing of 20 m, the computational region of 2 km by 2 km by 1 km in x-, y- and z-axes resulted in a model of size $101 \times 101 \times 51$. The source maximum frequency, the frequency interval, and the sampling rate were 10 Hz, 1 Hz, and 0.05 sec, respectively. The source was located at a depth of 10 m at the center of the model. With these parameters, the single CPU time to solve for a single frequency was about 80 minutes. This seems long in comparison to what might be achievable with finite-difference methods until one realizes that this would be the time required to generate data from a multiplicity of sources. Figs. 3 and 4 show the wavefront at 0.5 and 1 sec. In both figures, the vertical sections are taken at 1 km in the x and y directions, while the depth slice is at 0.1 km.

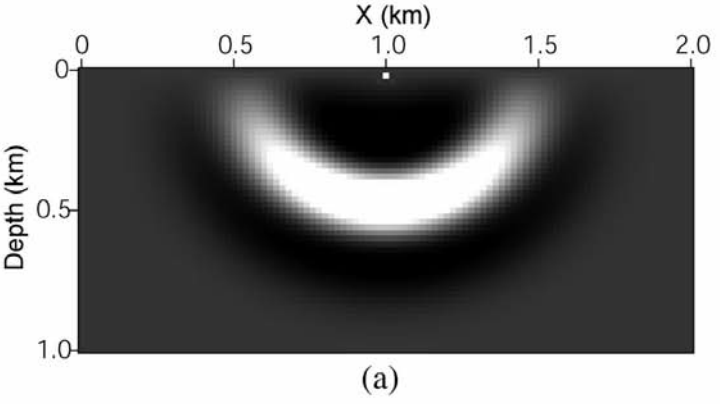

(a)

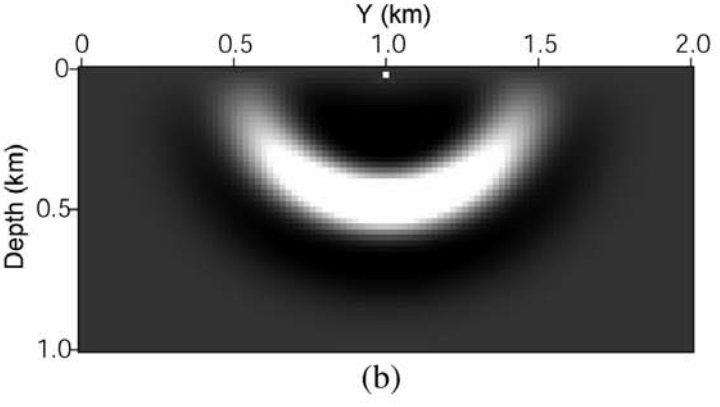

(b)

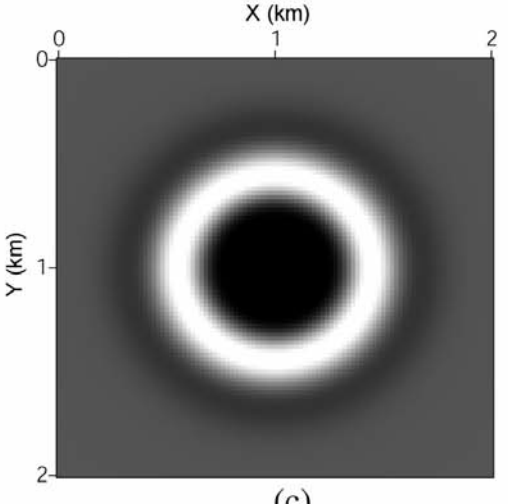

(c)

Fig. 3. Time slice section at 0.5 sec in (a) x-z plane when y = 1 km, (b) y-z plane when x = 1 km, and (c) x-y plane at the depth of 0.1 km.

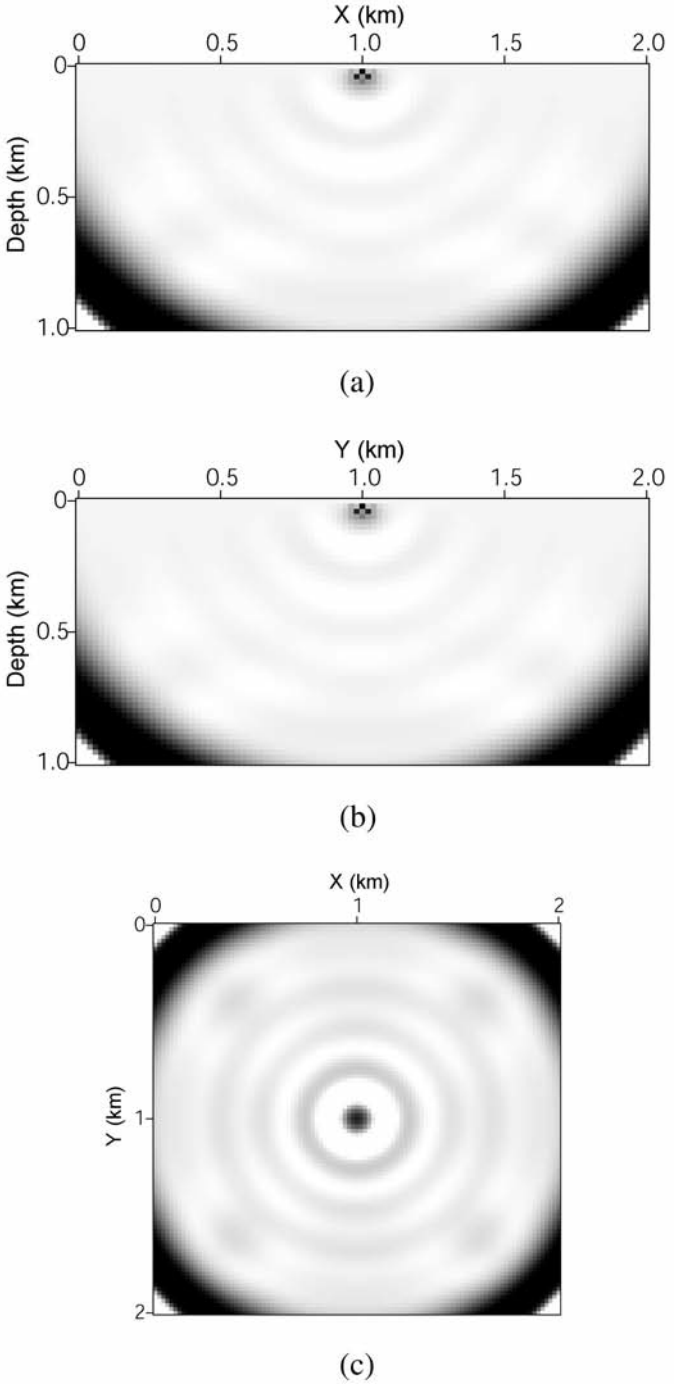

Fig. 4. Time slice section at 1 sec in (a) x-depth slice at y = 1 km, (b) y-depth slice at x = 1 km, and (c) x-y slice at the depth of 0.1 km.

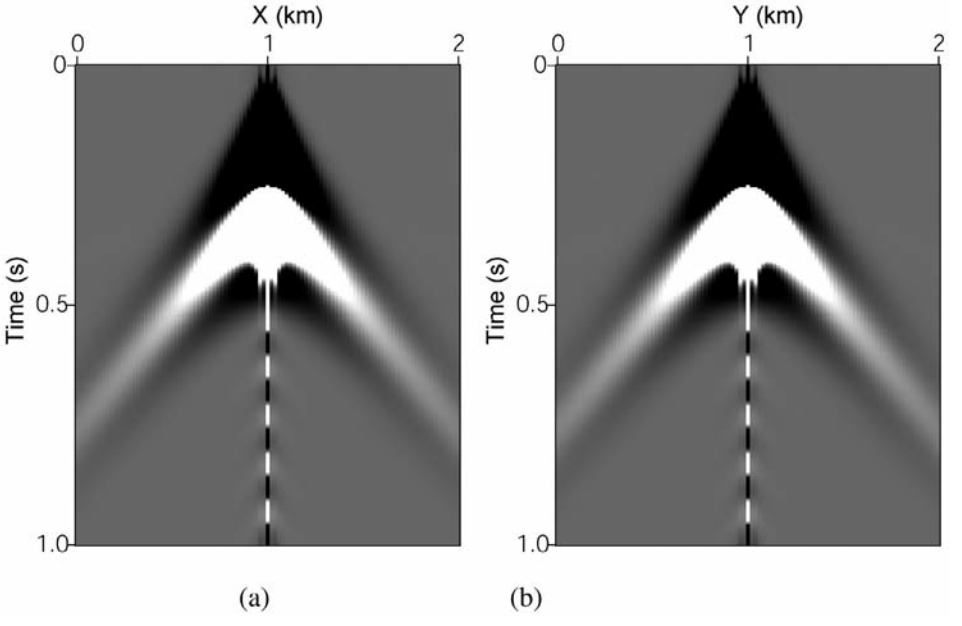

Fig. 5. Synthetic seismograms measured at the depth of 20 m along (a) the x line at y = 1 km and (b) the y line at x = 1 km.

Fig. 5 shows the seismogram observed at 20 m depth from the center on the surface. Fig. 5(a) represents the xz plane along the y = 1 km and Fig. 5(b) represents the yz plane along the x = 1 km. When the wave equation is solved in the frequency domain, there is a singular point corresponds to the shot position. In Fig. 5 and other figures of seismograms, the artifacts along vertical lines are caused by containing the signals of the singular point (the shot position). From Figs. 3, 4 and 5, note that the boundary conditions are working as required and that the waveforms show little or no dispersion. Fig. 6 compares traces obtained from centrally placed receivers at depths of 700 and 900 m.

Three layered model

Following the success of the simple experiment in the previous subsection, we generated a single synthetic wavefield using the three layered model shown in Fig. 7. The size of model is 3.2 × 3.2 × 1.6 km, and the model is sampled with the grid spacing of 60 m, which produces a spatial grid set of 161 × 161 × 81 nodes. Again, a source with a maximum frequency of 7.5 Hz was located

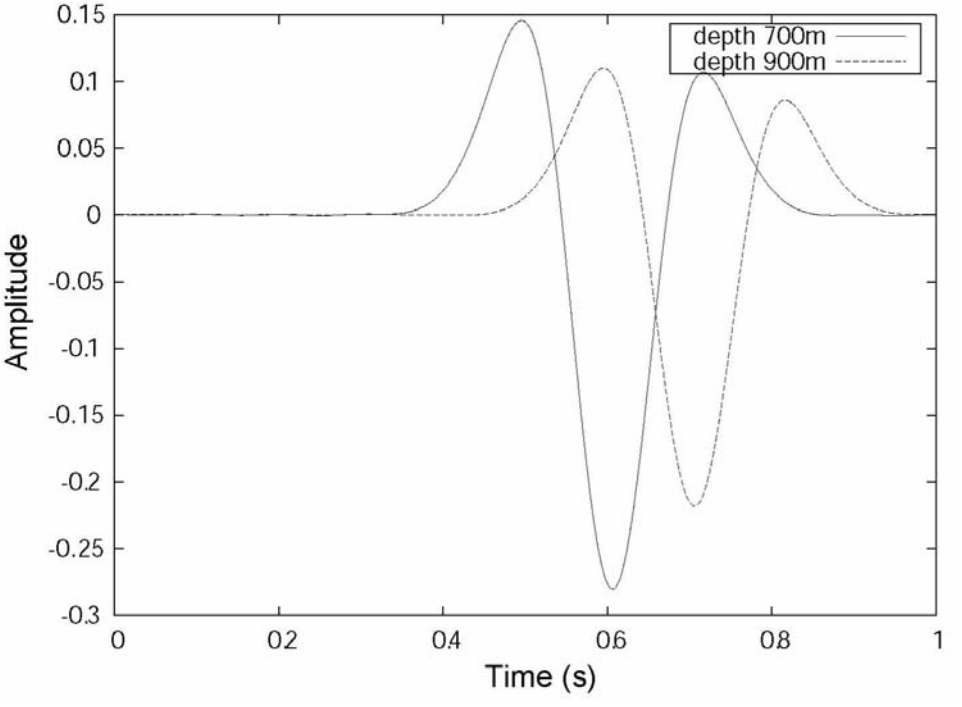

Fig. 6. Time trace obtained on the mid-point of xy plane at the depths of 700 m and 900 m.

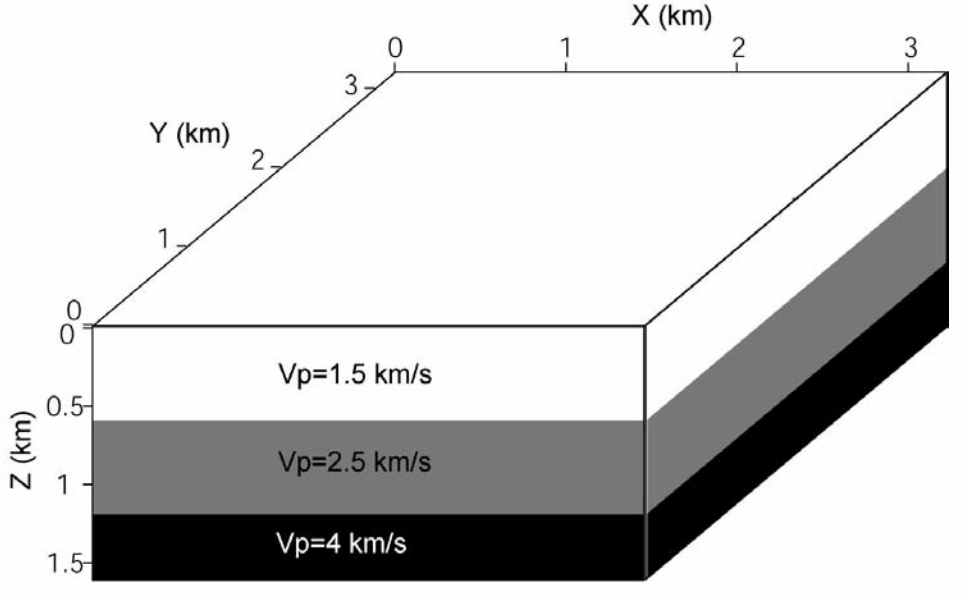

Fig. 7. Geometry of the 3 dimensional three layered model.

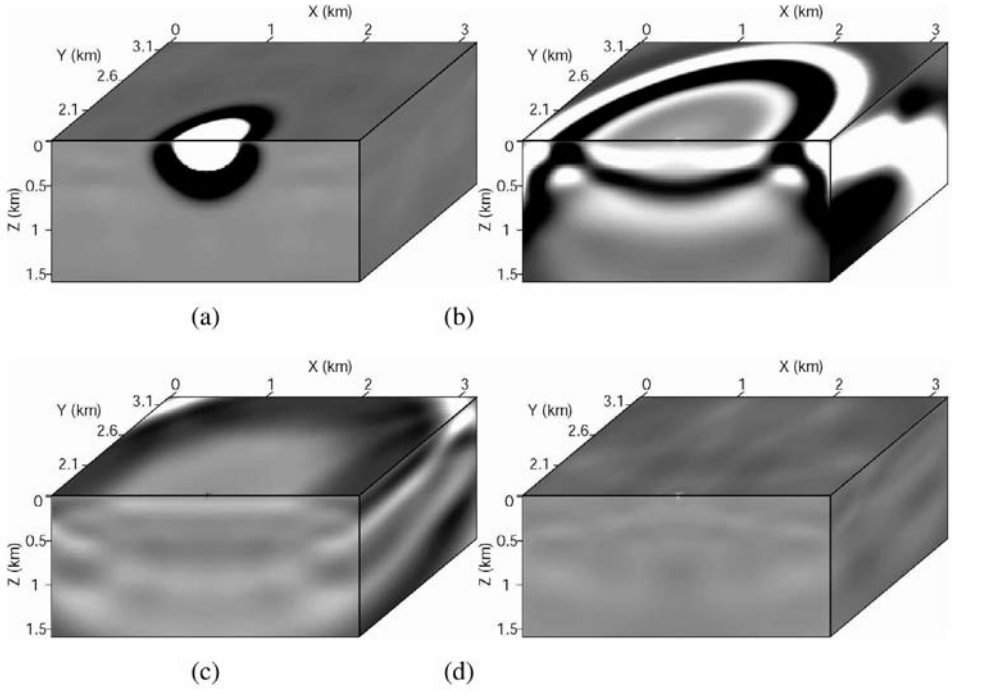

Fig. 8. Wave front by acoustic modeling for the 3 dimensional three layered model on a rectangular parallelepiped split by the x-z plane when y = 1.6 km at times of (a) 0.5, (b) 1.5, (c) 2.5 and (d) 3.5 sec.

at the center of the top surface at a depth of 20 m. The frequency interval and the sampling rate were 0.25 Hz and 0.0666 sec, respectively. In this case, it took 27 hours on 20 CPUs to perform the LU decomposition and generate 4 seconds of data. Fig. 8 shows three-dimensional views of wavefronts at 0.5, 1.5, 2.5 and 3.5 sec. Fig. 9 is a display of a vertical seismogram observed at a depth of 20 m at the center of the model. When we take the Fourier transform of the frequency-domain data into the time-domain, the 'wrapping around' effect, which occurs due to non-causal events leading the first arrival events, appears in the seismogram. In Fig. 9 and other figures of seismograms, we note that the 'wrapping around' effect appears.

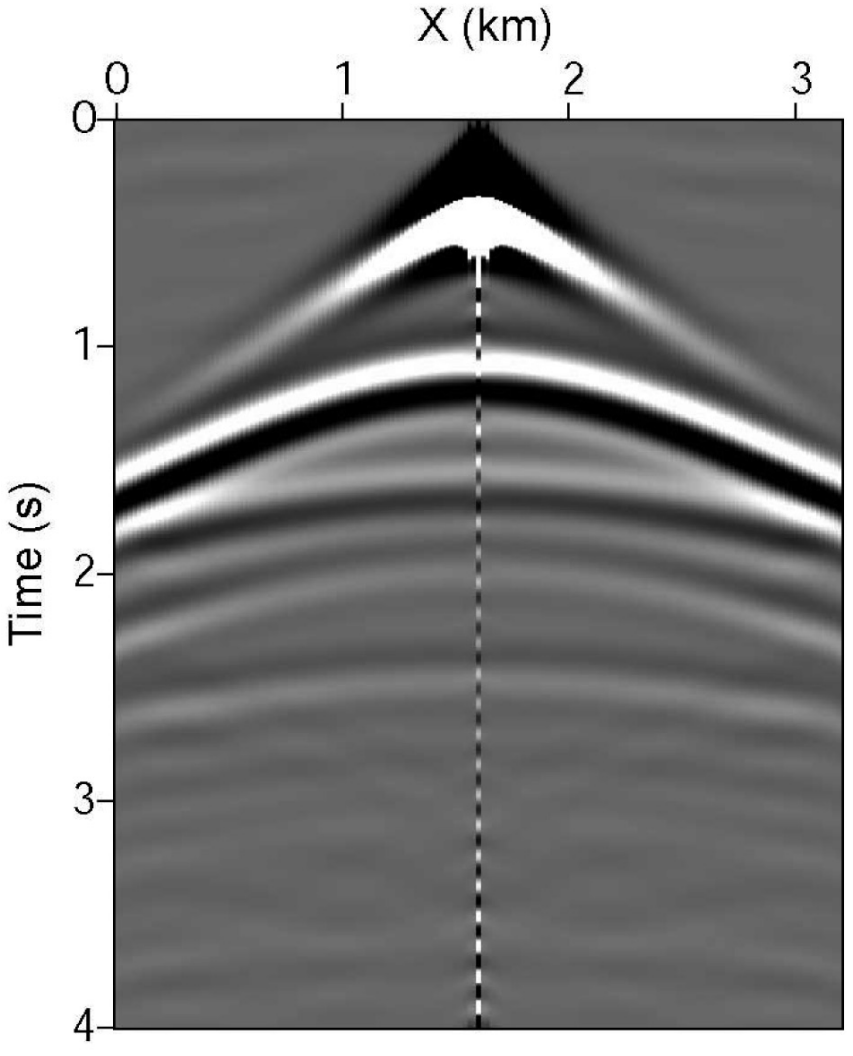

Fig. 9. Synthetic seismograms measured near the surface along the x line when y = 1.6 km.

SEG/EAGE 3D salt model

In our final example, we subsampled the 3D SEG/EAGE salt model to 60 m, producing a grid of 226 × 226 × 70 nodes. For this case, the maximum frequency of source, the frequency interval, and the sampling rate were 5 Hz, 0.125 Hz, and 0.1 sec, respectively. The approximate CPU time per frequency was 3600 minutes. Fig. 10 shows the velocity model and Figs. 11 and 12 show snapshots at 2, 4 and 6 sec. Fig. 13 shows seismograms from a source at a depth of 60 m at the center of the model's surface.

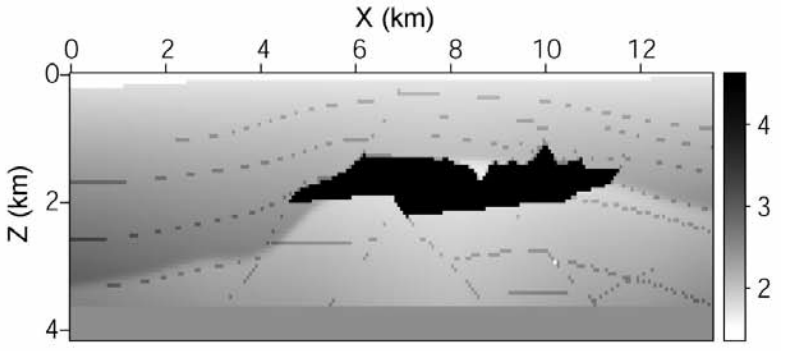

(a)

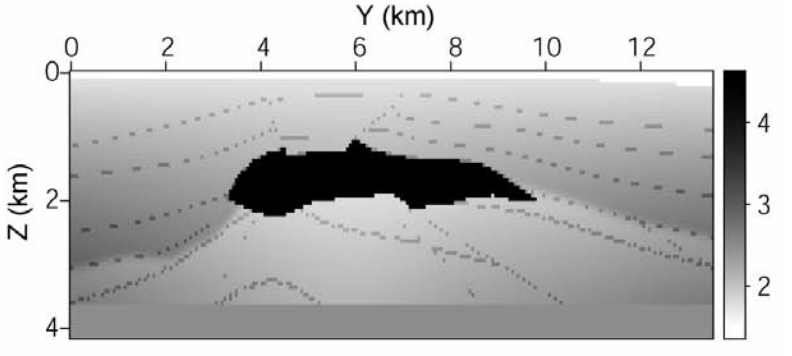

(b)

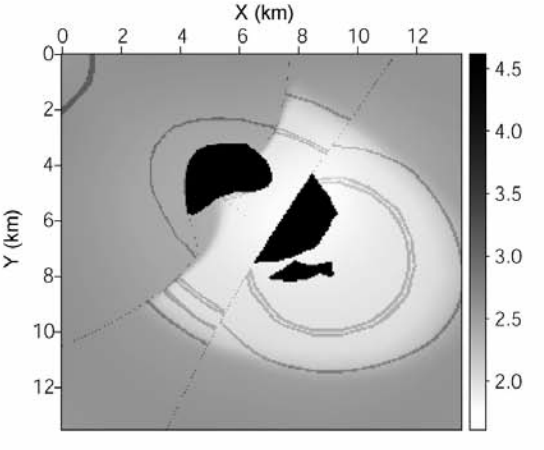

(c)

Fig. 10. 3D SEG/EAGE salt model. (a) x-z, (b) y-z, and (c) x-y slice section when y = 6.72 km, x = 6.72 km, and x = 2.1 km, respectively.

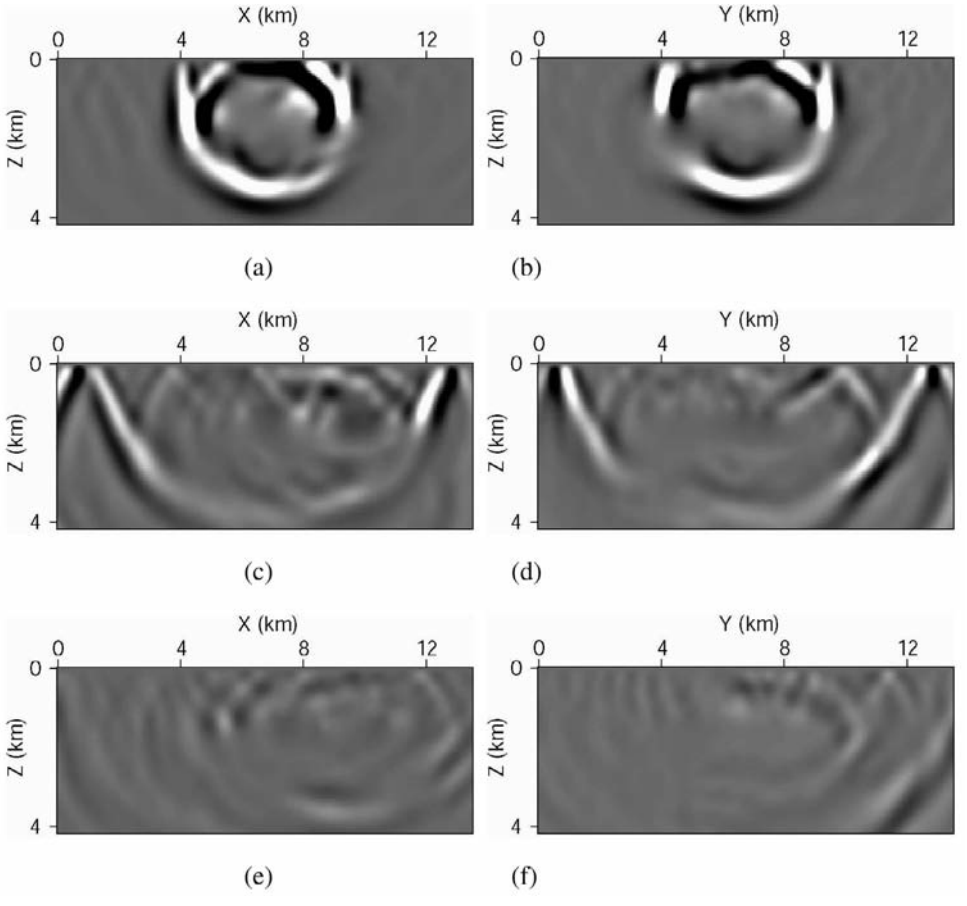

Fig. 11. Wave propagation for the 3D SEG/EAGE salt model on (a, c, e) the x-z plane at y = 6.72 km and (b, d, f) the y-z plane at x = 6.72 km at times of (a, b) 2, (c, d) 4 and (e, f) 6 sec.

CONCLUSION

We investigated three-dimensional frequency-domain modeling using the finite-element method. Although frequency-domain modeling requires a huge computer memory (especially in three dimensions), it has several advantages for waveform inversion over time-domain modeling. Multi-shot modeling, source estimation problem and parallel jobs for waveform inversion can be easily implemented in the frequency domain.

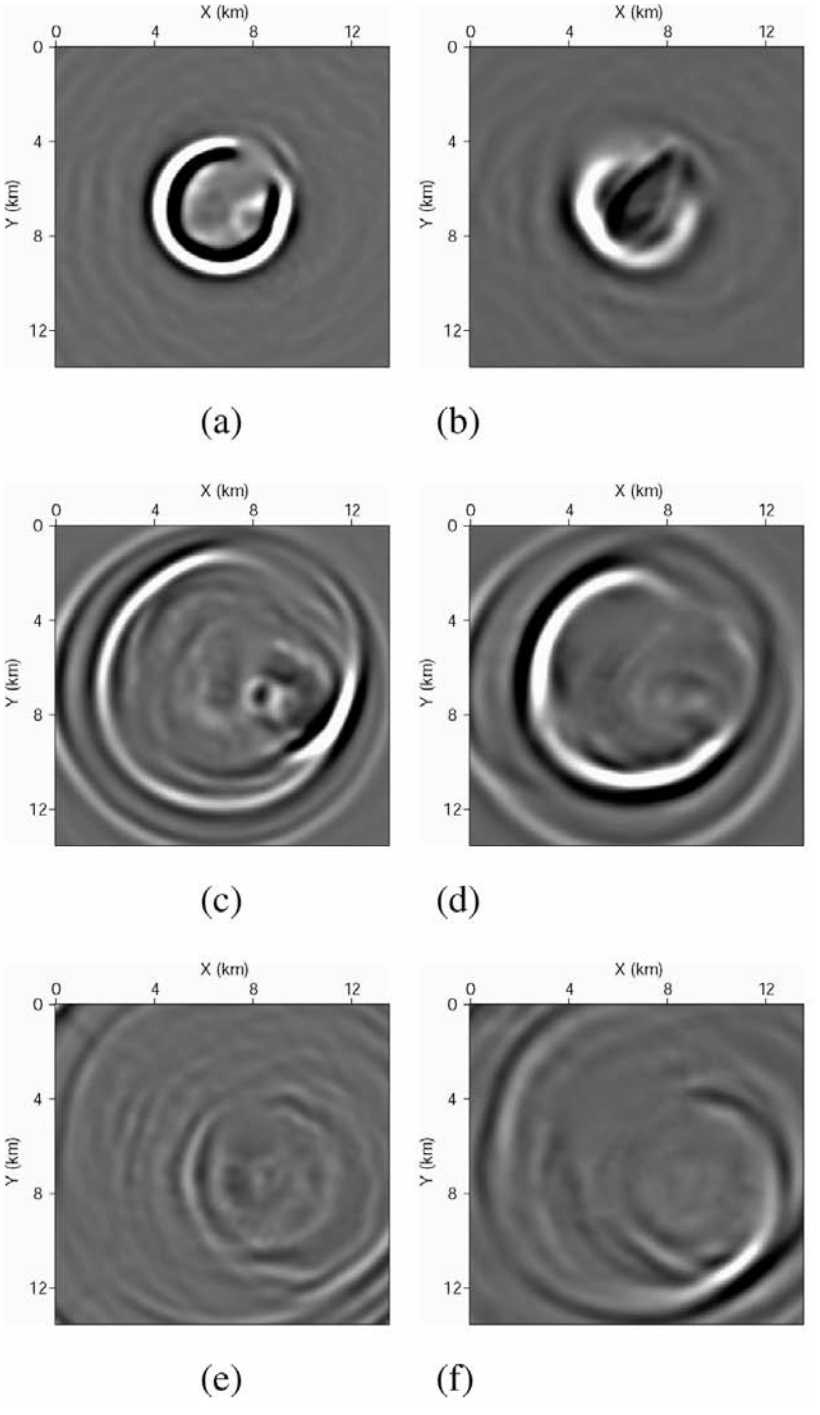

Fig. 12. Wave propagation for the 3D SEG/EAGE salt model on the x-y plane when (a, c, e) z = 1.2 km and (b, d, f) z = 2.4 km at times of (a, b) 2, (c, d) 4 and (e, f) 6 sec.

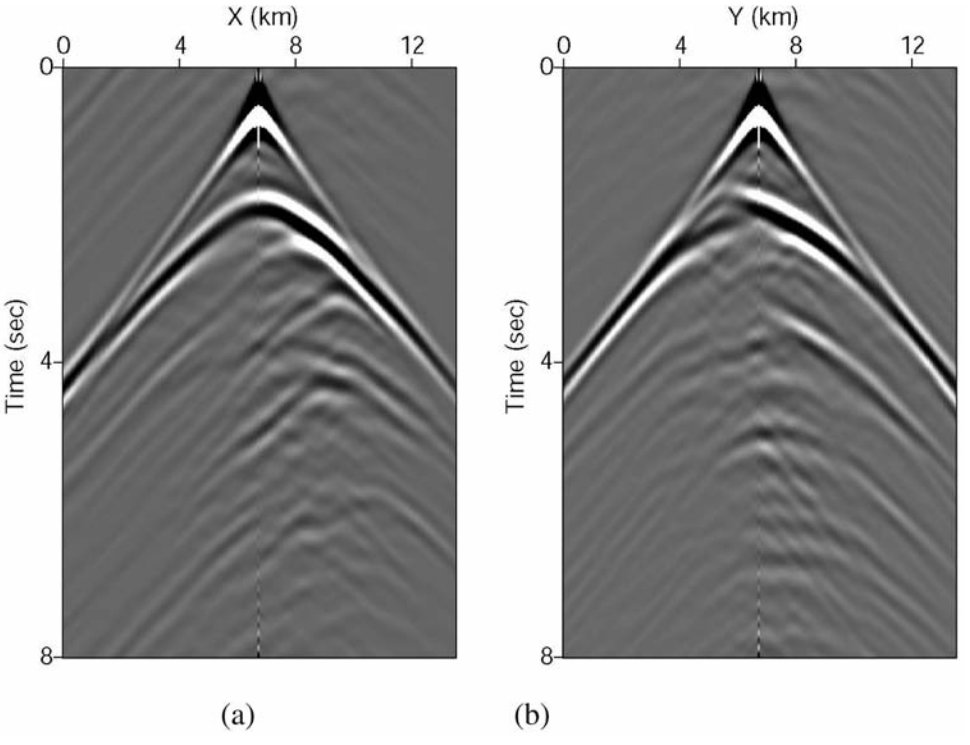

Fig. 13. Synthetic seismograms measured on the surface along (a) the x-axis when y = 6.72 km and (b) the y-axis when x = 6.72 km.

In this paper, we derived the numerical dispersion relationship for the 3D frequency-domain finite-element method and determined the minimum number of grid points per wavelength by dispersion analysis for 3D frequency-domain finite-element modeling. For unbounded boundary condition, we expanded Clayton and Engquist's 2D absorbing boundary condition to 3D and adapted this condition to the finite-element method. We validated the 3D frequency-domain modeling algorithm by applying it to homogeneous, three-layered and SEG/EAGE salt models. From the numerical experiments, we noted that the numerical results are little dispersive and the boundary condition works well. Using our computing capability, we proved that frequency-domain modeling is feasible even for large scale 3D models like the 3D SEG/EAGE salt model of 60 m. We feel that, in the near future, frequency-domain modeling for the 3D SEG/EAGE salt model of 20 m will be possible using the direct matrix solver with the advent of enhanced computer technology.

ACKNOWLEDGMENTS

This work was supported by Energy Technology Innovation (ETI) project funded by the Ministry of Knowledge Economy of the Korea, the Korea Science and Engineering Foundation (KOSEF) grant funded by the Korea government (MOST) (No. R0A-2006-000-10291-0), the Brain Korea 21 project of the Ministry of Education, and grant number PM50101 from the Korea Ocean Research and Development Institute. Shin's work was supported by the Korea Research Foundation Grant funded by the Korean Government (MOEHRD, Basic Research Promotion Fund (KRF-2006-311-D00987).

REFERENCES

Belytschko, T. and Mullen, R., 1990. On dispersive properties of finite element solution. In: Kelly, K.R. and Marfurt, K.J. (Eds.), Numerical Modeling of Seismic Wave Propagation, SEG, Tulsa, OK: 336-351.

Beylkin, G. and Sandberg, K., 2005. Wave propagation using bases for band limited functions: Wave Motion, 41: 263-291.

Carcione, J.M., Herman, G.C. and ten Kroode, A., 2002. Seismic modeling. Geophysics, 67: 1304-1325.

Claerbout, J.F., 1971. Toward a unified theory of reflector mapping. Geophysics, 36: 467-481.

Clayton, R. and Engquist, B., 1977. Absorbing boundary conditions for acoustic and elastic wave equations. Bull. Seismol. Soc. Am., 67: 1529-1540.

Kelly, K.R., Ward, R.W., Treitel, S. and Alford, R.M., 1976. Synthetic seismograms: a finite difference approach. Geophysics, 41: 2-27.

Marfurt, K.J., 1984. Accuracy of finite-difference and finite-element modeling of the scalar and elastic wave equations. Geophysics, 49: 533-549.

Officer, C.B., 1958. Introduction to the theory of Sound Transmission. McGraw-Hill, New York.

Pratt, R.G., Shin, C.S. and Hicks, G.J., 1998. Gauss-newton and full newton methods in frequency-space seismic waveform inversion. Geophys. J. Internat., 133: 341-362.

Reshef, M., Kosloff, D., Edwards, M. and Hsiung, C., 1988. Three-dimensional acoustic modeling by the Fourier method. Geophysics, 53: 1175-1183.

Shin, C. and Min, D., 2006. Waveform inversion using a logarithm wavefield. Geophysics, 71: R31-R42.

Shin, C., Yoon, K., Marfurt, K.J., Park, K., Yang, D., Lim, H., Chung, S. and Shin, S., 2001. Efficient calculation of a partial-derivative wavefield using reciprocity for seismic imaging and inversion. Geophysics, 66: 1856-1863.

Zienkiewicz, C. and Taylor, R.L., 2000. The finite element method. Vol. 1: The basis. 5th ed. Butterworth-Heinemann, Oxford.

APPENDIX A

HIGHER ORDER BOUNDARY CONDITION FOR 3D ACOUSTIC PROBLEMS

To assure stability of time extrapolation, based on equation (1) we consider the trial solutions

$$u(\mathbf{x},\omega) = \exp(ik_x x + ik_y y + ik_z z - i\omega t) \quad ,$$

from which we obtain the approximate dispersion relation

$$\omega = v(k_x^2 + k_y^2 + k_z^2)^{1/2} \quad . \tag{A-1}$$

Extrapolating in the z-direction produces

$$k_z = \pm(\omega/v)[1 - (v^2/\omega)(k_x^2 + k_y^2)^{1/2} \quad . \tag{A-2}$$

Using

$$\sqrt{(1 - x)} = 1 - \tfrac{1}{2}x + O(x^2) \quad , \tag{A-3}$$

we arrive at two approximations

$$(v/\omega)k_z = 1 + O[(v^2/\omega)^2(k_x^2 + k_y^2)] \quad , \tag{A-4a}$$

$$(v/\omega)k_z = 1 - \tfrac{1}{2}(v^2/\omega)^2(k_x^2 + k_y^2) + O[(v^2/\omega)^2(k_x^2 + k_y^2)] \quad , \tag{A-4b}$$

Using the Padé's method we get

$$a_j = 1 - [x/(1 + a_{j-1})] + O(x^2) \quad , \quad a_1 = 1 \quad , \tag{A-5}$$

and then obtain a third approximation

$$\begin{aligned}(v/\omega)k_z &= 1 - (v/\omega)^2(k_x^2 + k_y^2)/\{1 + [1 - \tfrac{1}{2}(v/\omega)^2(k_x^2 + k_y^2)]\} \\ &\quad + O[(v/\omega)^6(k_x^2 + k_y^2)^3] \quad , \\ &= 1 - (v/\omega)^2(k_x^2 + k_y^2)/[2 - \tfrac{1}{2}(v/\omega)^2(k_x^2 + k_y^2)] \\ &\quad + O[(v/\omega)^6(k_x^2 + k_y^2)^3] \quad , \\ &= [1 - (3/4)(v/\omega)^2(k_x^2 + k_y^2)]/[1 - (3/4)(v/\omega)^2(k_x^2 + k_y^2)] \\ &\quad + O[(v/\omega)^6(k_x^2 + k_y^2)^3] \quad .\end{aligned} \tag{A-6}$$

Rearranging eqs. (A-4) and (A-6), we get

$$A1 : k_z = \omega/v \quad , \tag{A-7a}$$

$$A2 : \omega k_z = (\omega^2/v) - \tfrac{1}{2}v(k_x^2 + k_y^2) \quad , \tag{A-7b}$$

$$A3 : v\omega^2 k_z - (1/4)v^3 k_z(k_x^2 + k_y^2) = \omega^3 - (3/4)\omega v^2(k_x^2 + k_y^2) \quad . \tag{A-7c}$$

Multiplying both sides of eq. (A-7) by $u = \exp(k_x x + k_y y + k_z z - i\omega t)$ yields

$$A1 : u_z = -(1/v)u_t \quad , \tag{A-8a}$$

$$A2 : u_{zt} = -(1/v)u_{tt} + (v/2)(u_{xx} + u_{yy}) \quad , \tag{A-8b}$$

$$A3 : -u_{ztt} + (v^2/4)(u_{zxx} + u_{zyy}) = (1/v)u_{ttt} + (3v/4)(u_{txx} + u_{tyy}) \quad . \tag{A-8c}$$

In the frequency domain, eq. (A-8) becomes

$$\dot{B}_1\tilde{u} = \tilde{u}_z - (i\omega/v)\tilde{u} = 0 \quad , \tag{A-9a}$$

$$\dot{B}_2\tilde{u} = \tilde{u}_z - (i\omega/v)\tilde{u} - (iv/2\omega)(\tilde{u}_{xx} + \tilde{u}_{yy}) = 0 \quad , \tag{A-9b}$$

$$\dot{B}_3\tilde{u} = \tilde{u}_z + (v^2/4\omega^2)(\tilde{u}_{zxx} + \tilde{u}_{zyy}) - i(\omega/v)\tilde{u} - (3iv/4\omega)(\tilde{u}_{xx} + \tilde{u}_{yy}) = 0 \quad . \tag{A-9c}$$

APPENDIX B

DISPERSION ANALYSIS FOR 3D ACOUSTIC PROBLEM

Our dispersion relation is obtained by setting the source term in eq. (3) to zero and ignoring the boundary condition (see also (Marfurt, 1984)). From eq. (6), the result is

$$-\omega^2 D_M\mathbf{u} - v^2 D_K\mathbf{u} = 0 \quad , \tag{B-1}$$

where $D_K = D_{xx} + D_{yy} + D_{zz}$ and

$$\begin{aligned} D_M\mathbf{u} = h^3[&(1/64)u_{i-1,j-1,k-1} + (1/32)u_{i-1,j,k-1} + (1/64)u_{i-1,j+1,k-1} + (1/32)u_{i-1,j-1,k} \\ &+ (1/16)u_{i-1,j,k} + (1/32)u_{i-1,j+1,k} + (1/64)u_{i-1,j-1,k+1} + (1/32)u_{i-1,j,k+1} \\ &+ (1/64)u_{i-1,j+1,k+1} + (1/32)u_{i,j-1,k-1} + (1/16)u_{i,j,k-1} + (1/32)u_{i,j+1,k-1} \end{aligned}$$

$$+ (1/16)u_{i,j-1,k} + (1/8)u_{i,j,k} + (1/16)u_{i,j+1,k} + (1/32)u_{i,j-1,k+1}$$
$$+ (1/16)u_{i,j,k+1} + (1/32)u_{i,j+1,k+1} + (1/64)u_{i+1,j-1,k-1} + (1/32)u_{i+1,j,k-1}$$
$$+ (1/64)u_{i+1,j+1,k-1} + (1/32)u_{i+1,j-1,k} + (1/16)u_{i+1,j,k} + (1/32)u_{i+1,j+1,k}$$
$$+ (1/64)u_{i+1,j-1,k+1} + (1/32)u_{i+1,j,k+1} + (1/64)u_{i+1,j+1,k+1}] \quad , \qquad \text{(B-2)}$$

$$D_{xx}\mathbf{u} = (h/3)[(1/12)u_{i-1,j-1,k-1} + (1/3)u_{i-1,j,k-1} + (1/12)u_{i-1,j+1,k-1} + (1/3)u_{i-1,j-1,k}$$
$$+ (4/3)u_{i-1,j,k} + (1/3)u_{i-1,j+1,k} + (1/12)u_{i-1,j-1,k+1} + (1/3)u_{i-1,j,k+1}$$
$$+ (1/12)u_{i-1,j+1,k+1} - (1/6)u_{i,j-1,k-1} - (2/3)u_{i,j,k-1} - (1/6)u_{i,j+1,k-1}$$
$$- (2/3)u_{i,j-1,k} - (8/3)u_{i,j,k} - (2/3)u_{i,j+1,k} - (1/6)u_{i,j-1,k+1}$$
$$- (2/3)u_{i,j,k+1} - (1/6)u_{i,j+1,k+1} + (1/12)u_{i+1,j-1,k-1} + (1/3)u_{i+1,j,k-1}$$
$$+ (1/12)u_{i+1,j+1,k-1} + (1/3)u_{i+1,j-1,k} + (4/3)u_{i+1,j,k} + (1/3)u_{i+1,j+1,k}$$
$$+ (1/12)u_{i+1,j-1,k+1} + (1/3)u_{i+1,j,k+1} + (1/12)u_{i+1,j+1,k+1}] \quad , \qquad \text{(B-3)}$$

and D_{yy} and D_{zz} are calculated similar to eq. (B-3). In a homogeneous medium, let $u_{l,m,n}$ be $\exp[i(k_x x_l + k_y y_m + k_y z_n)]$, so that eqs. (B-2) and (B-3) become

$$D_M\mathbf{u} = (h^3/8)\exp[i(k_x x_l + k_y y_m + k_y z_n)]$$
$$\times [\cos(k_x h) + 1][\cos(k_y h) + 1][\cos(k_z h) + 1] \quad , \qquad \text{(B-4)}$$

$$D_{xx}\mathbf{u} = (2/3)h\exp[i(k_x x_l + k_y y_m + k_y z_n)]$$
$$\times [\cos(k_x h) - 1][\cos(k_y h) + 2][\cos(k_z h) + 2] \quad , \qquad \text{(B-5)}$$

$$D_{yy}\mathbf{u} = (2/3)h\exp[i(k_x x_l + k_y y_m + k_y z_n)]$$
$$\times [\cos(k_x h) + 2][\cos(k_y h) - 1][\cos(k_z h) + 2] \quad , \qquad \text{(B-6)}$$

$$D_{zz}\mathbf{u} = (2/3)h\exp[i(k_x x_l + k_y y_m + k_y z_n)]$$
$$\times [\cos(k_x h) + 2][\cos(k_y h) + 2][\cos(k_z h) - 1] \quad , \qquad \text{(B-7)}$$

where h is the size of the spatial grid. In this case, eq. (B-1) becomes

$$-(\omega^2 h^3/8)[\cos(k_x h) + 1][\cos(k_y h) + 1][\cos(k_z h) + 1]$$

$$- (2v^2 h/3)\{[\cos(k_x h) - 1][\cos(k_y h) + 2][\cos(k_z h) + 2]$$

$$+ [\cos(k_x h) + 2][\cos(k_y h) - 1][\cos(k_z h) + 2] \ ,$$

$$+ [\cos(k_x h) + 2][\cos(k_y h) + 2][\cos(k_z h) - 1]\} = 0 \ . \quad \text{(B-8)}$$

Let θ be the azimuth, i.e., the angle that k forms with the k_x axis and φ be the angle that k forms with the k_z axis. Then, the relation between wave numbers and angles is as follows:

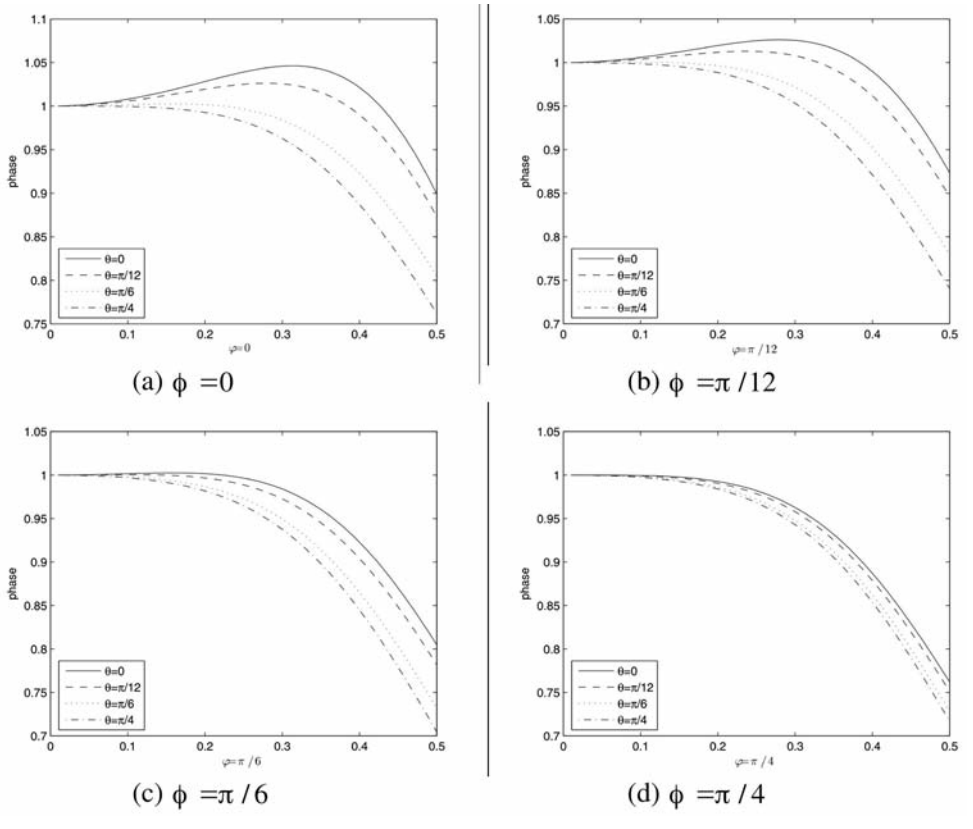

Fig. B-1. Dispersion analysis when θ = 0, $\pi/12$, $\pi/6$, and $\pi/4$ and = 0, $\pi/12$, $\pi/6$, and $\pi/4$.

$$k_x h = k\cos\varphi\cos\theta = (2\pi/G)\cos\varphi\cos\theta \quad , \tag{B-9}$$

$$k_y h = k\cos\varphi\sin\theta = (2\pi/G)\cos\varphi\sin\theta \quad , \tag{B-10}$$

$$k_z h = k\sin\varphi = (2\pi/G)\sin\varphi \quad , \tag{B-11}$$

where $k = 2\pi/\lambda$, λ is the wave length, and G denotes the grid points per wavelength. The phase velocity is

$$v/v_h = [1/(2\pi/G)]\sqrt{[(P_{xx} + P_{yy} + P_{zz})/P_m]} \quad , \tag{B-12}$$

where

$$P_m = (1/8)[1 + \cos(k_x h)][1 + \cos(k_y h)][1 + \cos(k_z h)] \quad , \tag{B-13}$$

$$P_{xx} = (2/9)[1 - \cos(k_x h)][2 + \cos(k_y h)][2 + \cos(k_z h)] \quad , \tag{B-14}$$

$$P_{yy} = (2/9)[2 + \cos(k_x h)][1 - \cos(k_y h)][2 + \cos(k_z h)] \quad , \tag{B-15}$$

$$P_{zz} = (2/9)[2 + \cos(k_x h)][2 + \cos(k_y h)][1 - \cos(k_z h)] \quad . \tag{B-16}$$

Fig. B-1, showing the dispersion relation at $\theta = 0, \pi/12, \pi/6, \pi/4$ and $\varphi = 0, \pi/12, \pi/6, \pi/4$, allows us to conclude that we need 5 grid points per wavelength to maintain a phase velocity dispersion error of less than 2%.